Available online at www.sciencedirect.com
SCIENCE DIRECT®
ELSEVIER
International Journal of Solids and Structures 41 (2004) 7287–7308
INTERNATIONAL JOURNAL OF SOLIDS and STRUCTURES
www.elsevier.com/locate/ijsolstr

Dynamical behaviors of nonlinear viscoelastic thick plates with damage

Dong-Fa Sheng [a,b], Chang-Jun Cheng [a,*]

[a] *Department of Mechanics, Shanghai Institute of Applied Mathematics and Mechanics, Shanghai University, Shanghai 200072, People's Republic of China*

[b] *Institute of Civil Engineering, Academy of Engineering Mechanics, Nanchang University, Nanchang 330029, People's Republic of China*

Received 6 June 2004
Available online 27 July 2004

Abstract

Based on the deformation hypothesis of Timoshenko's plates and the Boltzmann's superposition principles for linear viscoelastic materials, the nonlinear equations governing the dynamical behavior of Timoshenko's viscoelastic thick plates with damage are presented. The Galerkin method is applied to simplify the set of equations. The numerical methods in nonlinear dynamics are used to solve the simplified systems. It could be seen that there are plenty of dynamical properties for dynamical systems formed by this kind of viscoelastic thick plate with damage under a transverse harmonic load. The influences of load, geometry and material parameters on the dynamical behavior of the nonlinear system are investigated in detail. At the same time, the effect of damage on the dynamical behavior of plate is also discussed.

Keywords: Viscoelastic solid with damage; Thick plate; Geometrical non-linearity; Stability; Chaos; Bifurcation; Parameter study

1. Introduction

With the increasing use of viscoelastic materials in the national defence and civilian industry, the theory of viscoelasticity has absorbed many researchers' attention and becomes one of important branches in solid mechanics. Due to large deformations and/or nonlinear constitutive relations to make the mathematical model of the problem becomes nonlinear and hence bifurcation and chaos might occur. With the development of the mathematical theory of bifurcation and chaos, there are a lot of reports about the chaos motion of viscoelastic structures. Touati and Cederbaum (1995) used the history curve, power spectrum and the largest Liapunov exponent to numerically study the chaotic motion of nonlinear viscoelastic plates under small deflection. Later, they used the phase diagram, Poincare section, power spectrum and the

* Corresponding author. Tel./fax: +86-21-5638-0560.
E-mail addresses: shengdf@eyou.com (D.-F. Sheng), chjcheng@yc.shu.edu.cn (C.-J. Cheng).

0020-7683/$ - see front matter © 2004 Elsevier Ltd. All rights reserved.
doi:10.1016/j.ijsolstr.2004.06.011

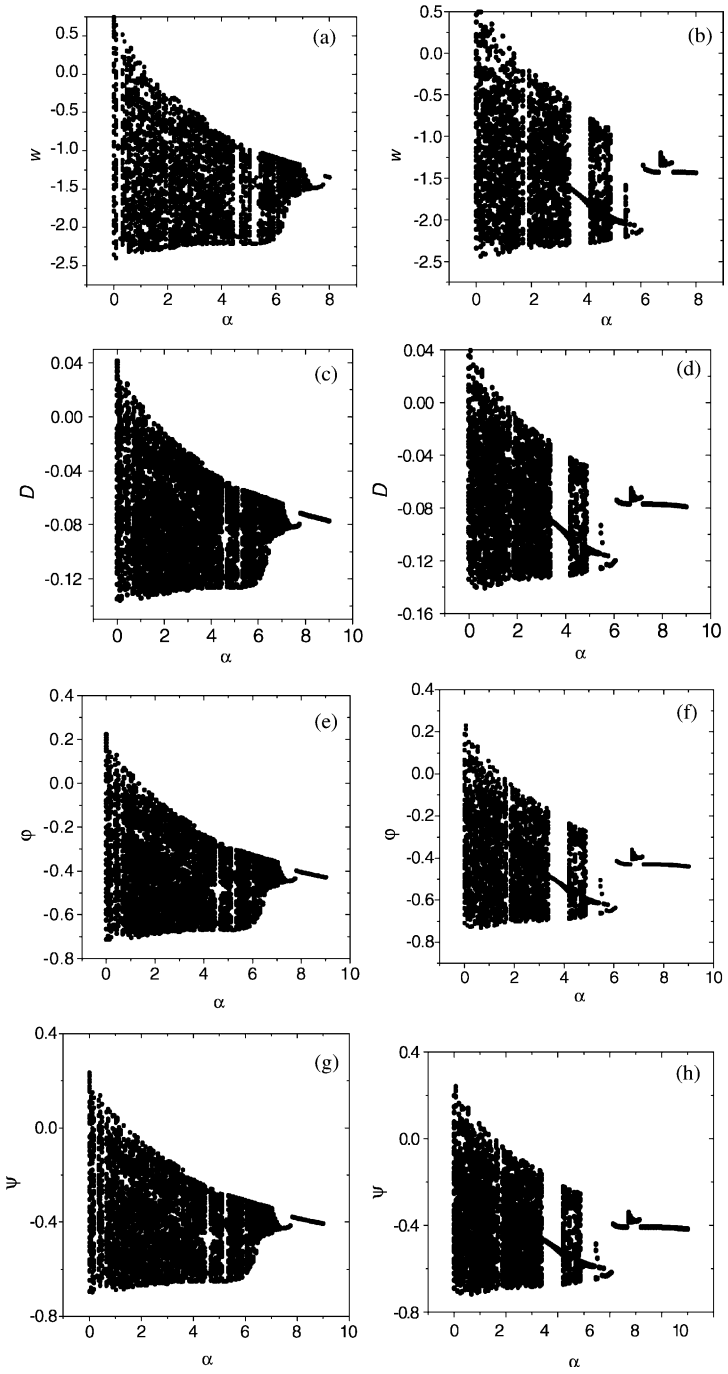

Fig. 1. Bifurcation figures of deflection, damage increase and rotation angles for different loads and $\beta_1 = 10$: (a) $q = 0.02$, (b) $q = 0.021$, (c) $q = 0.02$, (d) $q = 0.021$, (e) $q = 0.02$, (f) $q = 0.021$, (g) $q = 0.02$, (h) $q = 0.021$.

largest Liapunov exponent to numerically study the chaos motion of nonlinear viscoelastic plates under large deflection. Suire and Cederbaum (1995) analyzed periodic and chaotic behavior of viscoelastic beams

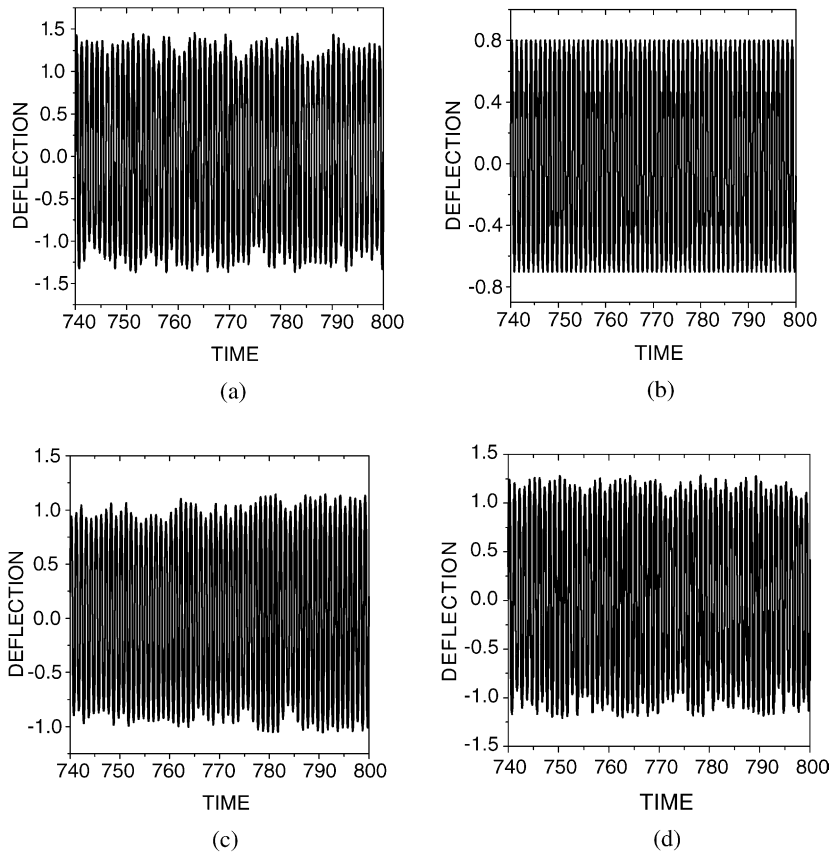

Fig. 2. Time-path curves of deflection for $\alpha = 0.2$, $q = 0.2$: (a) $\beta_1 = 4.2$, (b) $\beta_1 = 4$, (c) $\beta_1 = 3.8$, (d) $\beta_1 = 3.5$.

with the large deflection in which they adopted the Boltzmann superposition principle as the constitutive relation. Argyris (1996) investigated the chaotic motion of viscoelastic beams based on differential-type constitutive relation. Recently, Ding et al. (1998) studied the dynamic properties of nonlinear viscoelastic plates. Zhu et al. (1998) investigated the chaotic behavior of viscoelastic rectangular plates under large deflection. Cheng and Zhang (1998) used the history curve, phase trajectory diagram, stroboscopic observation and Liapunov exponent spectrum to analyze dynamical behavior of viscoelastic plates under large deflection and found the hyper-chaos phenomena. And they showed that the motion states alternate between chaos and hyperchaos for larger load amplitude. Li et al. (2002) analyzed the dynamic behaviors of viscoelastic plates with finite deformation and higher-order shear deformation effects based on Reddy's theory of plates and Boltzmann superposition principles. At the same time, there are a lot of papers on the stability of viscoelastic structures (see e.g. Tylikowski, 1989; Drozdov, 1993; Parker and Chua, 1989; Cederbaum and Aboudi, 1991; Cederbaum and Mond, 1992; Cederbaum and Drawshi, 1994). But the authors have not found reports on the dynamical behaviors of nonlinear viscoelastic structures with damage.

The dynamic response of mechanical and civil structures subjected to high-amplitude motions is often dangerous and undesirable. Nonlinear vibration is the most detrimental form of the motions. All mechanical systems subjected to various conditions may result in vibrational motion, which often lead to material fatigue, structural damage and failure, deterioration of system performance, and increased noise

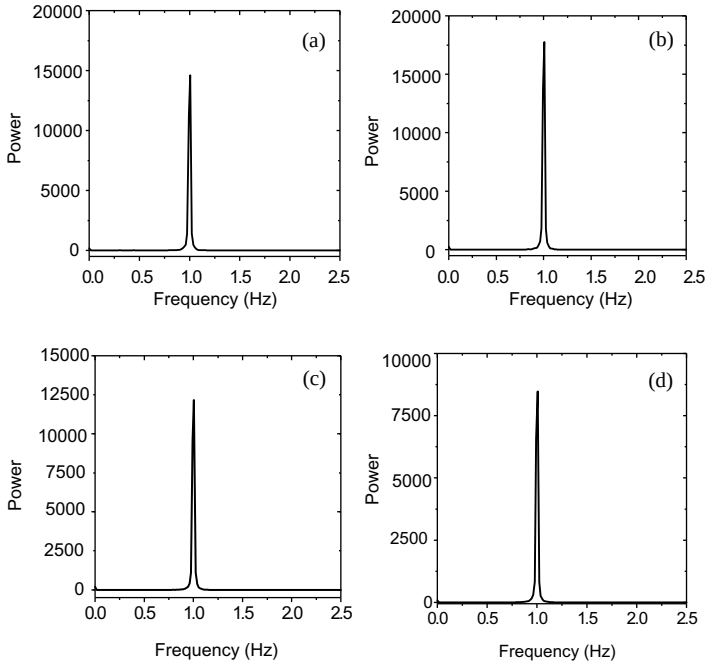

Fig. 3. Power spectrums of deflection for $\alpha = 0.2$, $q = 0.2$: (a) $\beta_1 = 4.2$, (b) $\beta_1 = 4$, (c) $\beta_1 = 3.8$, (d) $\beta_1 = 3.5$.

level. Large amplitude vibration phenomenon of a plate plays an important role in modern science and technology. In this paper, based on the Timoshenko's finite deformation hypothesis of thick plates and Boltzmann superposition principle of viscoelastic materials, a set of nonlinear equations governing dynamical behaviors of viscoelastic thick plates with damage are derived from the theory of plates with finite deformations under the assumption that the damage increment is a thrice function of coordinate z. One can see that the derived equations are a set of nonlinear integro-partial-differential equations. It is not easy to obtain the solution of equations. Here, we first apply the Galerkin method to simplify the set of equations into a set of integro-ordinary-differential equations. Then, the dynamic behaviors of the first-order and second-order truncated systems are numerically studied by the use of the methods in nonlinear dynamics. The influences of the load, geometry and material parameters on the dynamic behaviors of the nonlinear viscoelastic plates with damage are considered in detail. Results indicate that there are plenty of dynamic properties of both the damage increment and displacements for the kind of the dynamical systems and their dynamic behaviors of the damage increment and displacements are similar. At the same time, we also review the effect of damage on dynamic properties of the plate.

2. Mathematical model of viscoelastic plates with damage and its simplification

2.1. Dynamical equations of viscoelastic solids with damage

Let u_i, ε_{ij}, σ_{ij} and Đ be displacement, strain, stress components and damage field respectively, all of them are functions of coordinate x_i and time t. According to basic rules of continuum damage mechanics, the

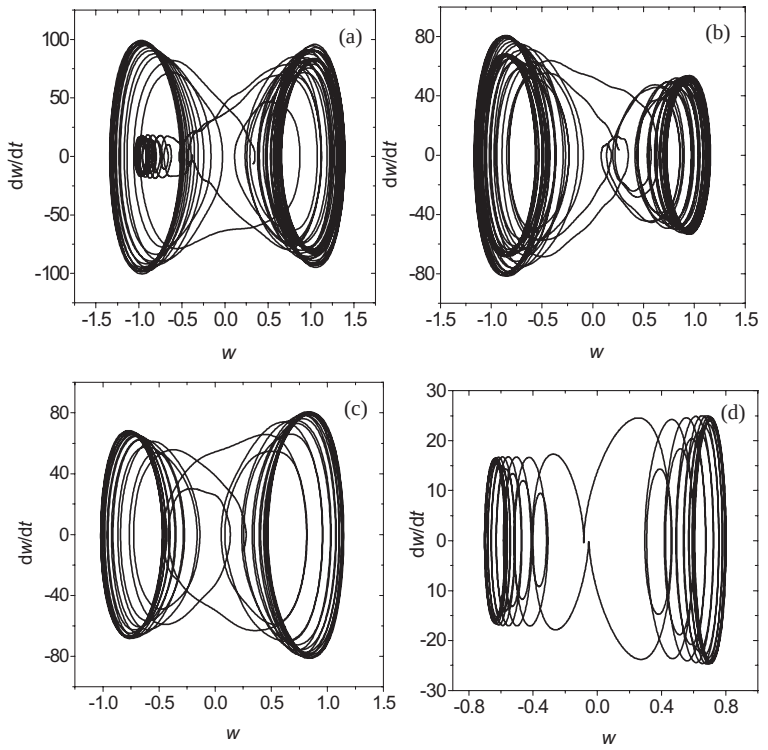

Fig. 4. Phase-trajectory diagrams of deflection for $\alpha = 0.2$, $q = 0.2$: (a) $\beta_1 = 4.2$, (b) $\beta_1 = 4$, (c) $\beta_1 = 3.8$, (d) $\beta_1 = 3.5$.

above variables satisfy the following equations in the case of finite deformations (see e.g. Cowin and Nunziato, 1983).

Differential equations of motion

$$\sigma_{ij,j} + f_i - \rho\ddot{u}_i = 0, \tag{1}$$

$$\rho k\ddot{\text{Đ}} - \alpha \text{Đ}_{,ii} + \omega \text{Đ} + \xi(\text{Đ} - \text{Đ}^0) - \beta\varepsilon_{kk} + l = 0. \tag{2}$$

Geometry equations

$$\varepsilon_{ij} = \frac{1}{2}\left(u_{i,j} + u_{j,i} + \frac{\partial u_k}{\partial x_i}\frac{\partial u_k}{\partial x_j}\right). \tag{3}$$

Constitutive equations

$$\sigma_{ij} = C_1 \otimes \varepsilon_{ij} + C_2 \otimes \varepsilon_{kk}\delta_{ij} - \beta(\text{Đ} - \text{Đ}^0)\delta_{ij}. \tag{4}$$

In (1)–(4), f_i is the known body force, ρ known density in the reference configuration, k the known equilibrated inertia, l the known extrinsic equilibrated body force, α, ω, ξ, β are respectively material coefficients and Đ^0 represents the initial damage field. In addition, the constitutive functions of viscoelastic materials, denoted C_1 and C_2, are given by $C_1 = L^{-1}\left[1/\left(s^2\overline{J}_1\right)\right]$, $C_2 = L^{-1}\left[\left(\overline{J}_1 - \overline{J}_2\right)/s^2\overline{J}_1\left(\overline{J}_1 + 2\overline{J}_2\right)\right]$, where J_1 and J_2 are the creep functions. $\overline{(\cdot)}$ and L^{-1} express Laplace transformation and its inverse transformation, s is a transformation parameter. The symbol $\otimes$ indicates Boltzmann operator defined by

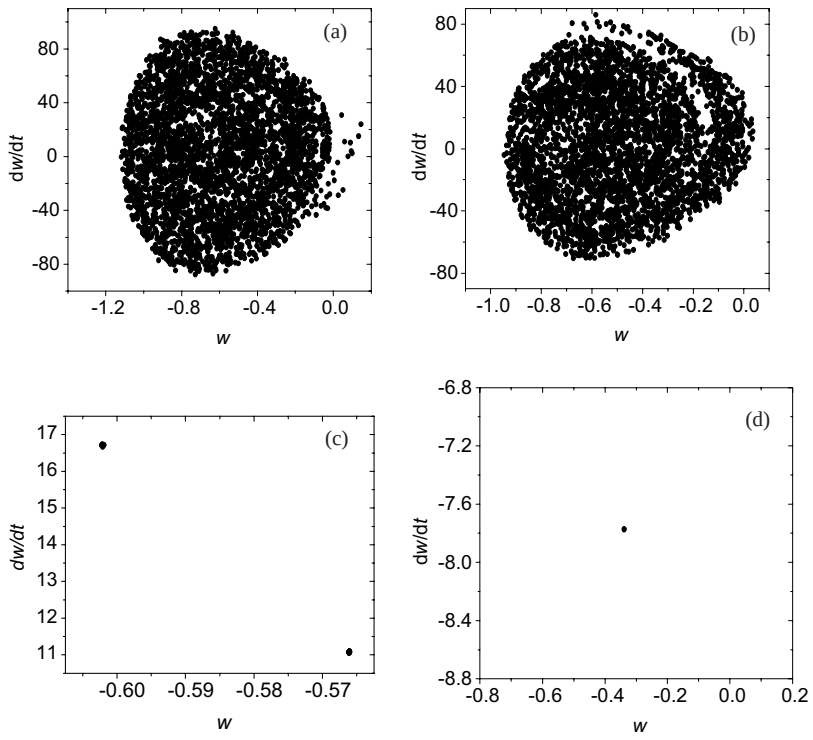

Fig. 5. Poincare sections of deflection for $\alpha = 0.2$, $q = 0.2$: (a) $\beta_1 = 4.2$, (b) $\beta_1 = 4$, (c) $\beta_1 = 3.8$, (d) $\beta_1 = 3.5$.

$$\varphi_1(t) \otimes \varphi_2(t) = \varphi_1(0^+)\varphi_2(t) + \dot{\varphi}_1(t) \ * \ \varphi_2(t) = \varphi_1(0^+)\varphi_2(t) + \int_{0^+}^{t} \dot{\varphi}_1(t-\tau)\varphi_2(\tau)\,\mathrm{d}\tau.$$

2.2. Mathematical model of viscoelastic plates with damage

Assume that h is the thickness of the plate and that the plate is subjected to a transverse harmonic load $q(x, y, t)$. Let u, v and w be the displacements in the x, y, z directions, φ and ψ are rotations of the normal of the mid-plane about the x and y axes, respectively. Based on the Timoshenko's deformation geometry hypothesis of thick plates, u, v and w could be expressed as

$$\left.\begin{aligned} u(x,y,z,t) &= u^0(x,y,t) - z\varphi(x,y,t) \\ \upsilon(x,y,z,t) &= \upsilon^0(x,y,t) - z\psi(x,y,t) \\ w(x,y,z,t) &= w^0(x,y,t) \end{aligned}\right\} \tag{5}$$

in which, u^0, υ^0 and w^0 are the mid-plane displacements in the x, y, z directions, respectively.

If the rotations are lager, from the von Kármán's theory, the thick plate's strains may be decomposed into two parts, that is, the average strains and bending strains, they are given as (see e.g. Cheng and Zhu, 1991)

$$\varepsilon_x = \varepsilon_x^0 - z\varphi_{,x}, \quad \varepsilon_y = \varepsilon_y^0 - z\psi_{,y}, \quad \gamma_{xy} = \gamma_{xy}^0 - z(\varphi_{,y} + \psi_{,x}), \quad \gamma_{xz} = w_{,x} - \varphi, \quad \gamma_{yz} = w_{,y} - \psi \tag{6}$$

in which, ε_x^0, ε_y^0 and γ_{xy}^0 are average strains expressed as

$$\varepsilon_x^0 = u_{,x}^0 + w_{,x}^2/2, \quad \varepsilon_y^0 = \upsilon_{,y}^0 + w_{,y}^2/2, \quad \gamma_{xy}^0 = u_{,y}^0 + \upsilon_{,x}^0 + w_{,x}w_{,y}. \tag{7}$$

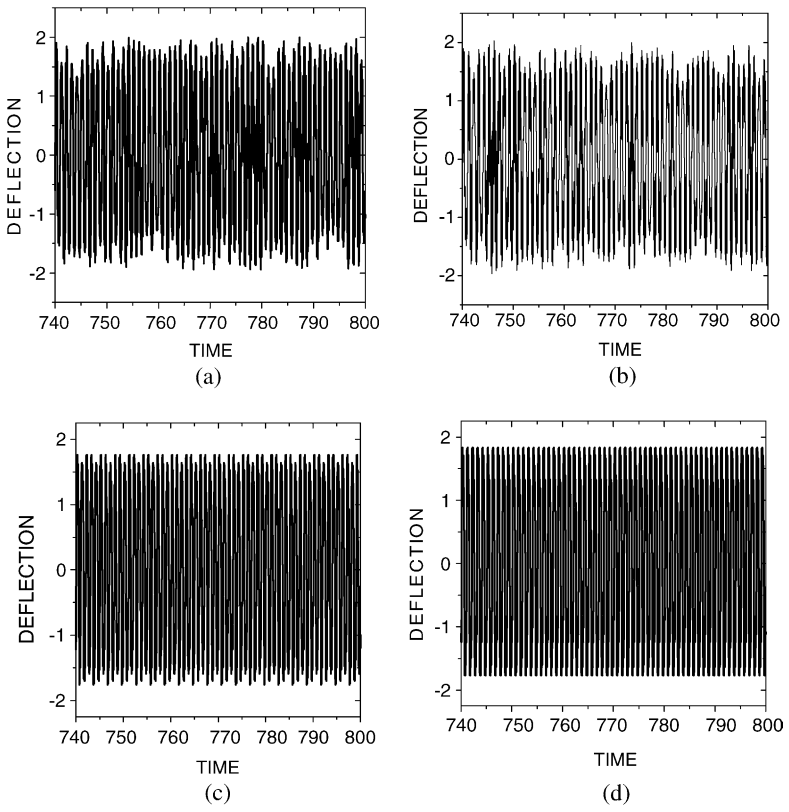

Fig. 6. Time-path curves of deflection for $\beta_1 = 10$: (a) $\alpha = 0.02$, (b) $\alpha = 0.2$, (c) $\alpha = 5.0$, (d) $\alpha = 10.0$.

For convenience and certainty, assume that the damage increment is a thrice function of coordinate z, namely,

$$\text{Đ}(x_i, t) - \text{Đ}^0(x_i) = D(x_\alpha, t)\left(\frac{z^3}{3} - \frac{h^2}{4}z\right). \tag{8}$$

Clearly, the damage increment function satisfies the condition at the surfaces $z = \pm\frac{h}{2}$ (see e.g. Cowin and Nunziato, 1983). Here and henceforth, we adopt the conventional regulation, namely, Greek letters represent x and y only. Substituting into (1) yields

$$\begin{aligned}
\sigma_x &= (C_1 + C_2) \otimes \left(\varepsilon_x^0 - z\varphi_{,x}\right) + C_2 \otimes \left(\varepsilon_y^0 - z\psi_{,y}\right) - \beta D\left(\frac{z^3}{3} - \frac{h^2}{4}z\right),\\
\sigma_y &= C_2 \otimes \left(\varepsilon_x^0 - z\varphi_{,x}\right) + (C_1 + C_2) \otimes \left(\varepsilon_y^0 - z\psi_{,y}\right) - \beta D\left(\frac{z^3}{3} - \frac{h^2}{4}z\right),\\
\tau_{xy} &= \frac{1}{2}C_1 \otimes \left[\gamma_{xy}^0 - z(\varphi_{,y} + \psi_{,x})\right],\\
\tau_{xz} &= \frac{1}{2}C_1 \otimes (w_{,x} - \varphi), \quad \tau_{yz} = \frac{1}{2}C_1 \otimes (w_{,y} - \psi).
\end{aligned} \tag{9}$$

The internal force components can be expressed as

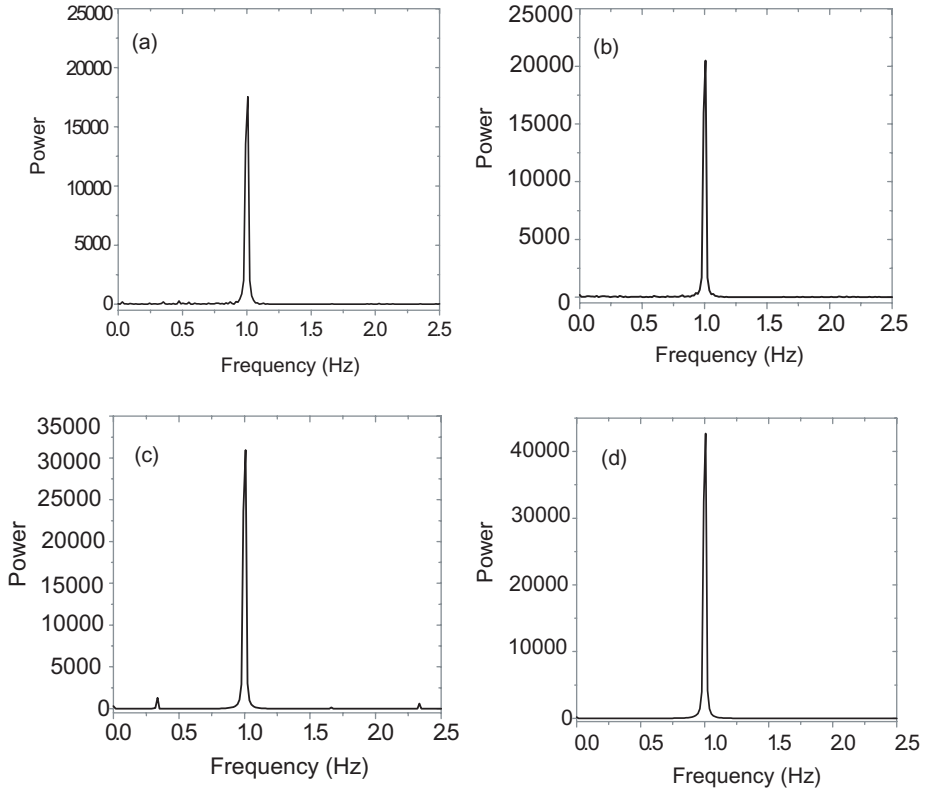

Fig. 7. Power spectrums of deflection for $\beta_1 = 10$, $q = 0.01$: (a) $\alpha = 0.02$, (b) $\alpha = 0.2$, (c) $\alpha = 5.0$, (d) $\alpha = 10.0$.

$$
\begin{aligned}
N_x &= \int_{-h/2}^{h/2} \sigma_x \,\mathrm{d}z = h\left[(C_1 + C_2) \otimes \left(u^0_{,x} + w^2_{,x}/2\right) + C_2 \otimes \left(v^0_{,y} + w^2_{,y}/2\right)\right], \\
N_y &= \int_{-h/2}^{h/2} \sigma_y \,\mathrm{d}z = h\left[C_2 \otimes (u^0_{,x} + w^2_{,x}/2) + (C_1 + C_2) \otimes \left(v^0_{,y} + w^2_{,y}/2\right)\right], \\
N_{xy} &= \int_{-h/2}^{h/2} \tau_{xy} \,\mathrm{d}z = \frac{h}{2} C_1 \otimes \left(u^0_{,y} + v^0_{,x} + w_{,x} w_{,y}\right), \\
Q_x &= \int_{-h/2}^{h/2} \tau_{xz} \,\mathrm{d}z = \frac{h}{2} C_1 \otimes (w_{,x} - \varphi), \\
Q_y &= \int_{-h/2}^{h/2} \tau_{yz} \,\mathrm{d}z = \frac{h}{2} C_1 \otimes (w_{,y} - \psi), \\
M_x &= \int_{-h/2}^{h/2} \sigma_x z \,\mathrm{d}z = -\frac{h^3}{12}\left[(C_1 + C_2) \otimes \varphi_{,x} + C_2 \otimes \psi_{,y} - \frac{h^2}{5}\beta D\right], \\
M_y &= \int_{-h/2}^{h/2} \sigma_y z \,\mathrm{d}z = -\frac{h^3}{12}\left[C_2 \otimes \varphi_{,x} + (C_1 + C_2) \otimes \psi_{,y} - \frac{h^2}{5}\beta D\right], \\
M_{xy} &= \int_{-h/2}^{h/2} \tau_{xy} z \,\mathrm{d}z = -\frac{h^3}{24} C_1 \otimes (\varphi_{,y} + \psi_{,x})
\end{aligned}
\tag{10}
$$

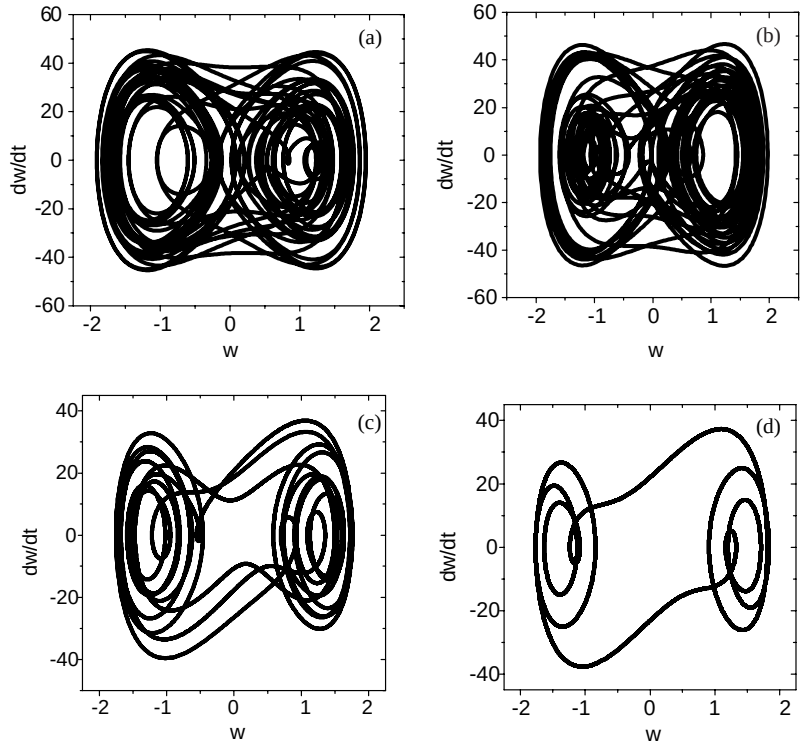

Fig. 8. Phase-trajectory diagrams of deflection for $\beta_1 = 10$, $q = 0.01$: (a) $\alpha = 0.02$, (b) $\alpha = 0.2$, (c) $\alpha = 5.0$, (d) $\alpha = 10.0$.

in which, N_x, N_y and $N_{xy} = N_{yx}$ are the internal forces acting on the mid-plane of the plate, separately, and Q_x, Q_y, M_x, M_y and $M_{xy} = M_{yx}$ are the transverse shearing forces, bending moments and torques of the plate.

It would be assumed that the inertia force on the mid-plane could be ignored. From the equilibrium of the plate, we can yield a sets of differential equations of motion in terms of five displacements, that is, the displacements u^0, v^0, $w^0 = w$ and rotation angles φ, ψ

$$
\begin{aligned}
&(C_1 + C_2) \otimes (u^0_{,xx} + w_{,x} w_{,xx}) + C_2 \otimes (v^0_{,yx} + w_{,y} w_{,yx}) + \frac{1}{2} C_1 \otimes \left(u^0_{,yy} + v^0_{,xy} + w_{,xy} w_{,y} + w_{,x} w_{,yy} \right) = 0, \\
&C_2 \otimes \left(u^0_{,xy} + w_{,x} w_{,xy} \right) + (C_1 + C_2) \otimes \left(v^0_{,yy} + w_{,y} w_{,yy} \right) + \frac{1}{2} C_1 \otimes \left(u^0_{,yx} + v^0_{,xx} + w_{,xx} w_{,y} + w_{,x} w_{,yx} \right) = 0, \\
&h \Bigg\{ \frac{1}{2} C_1 \otimes (\nabla^2 w - \varphi_{,x} - \psi_{,y}) + \Bigg[(C_1 + C_2) \otimes \left(u^0_{,xx} + w_{,x} w_{,xx} \right) + C_2 \otimes \left(v^0_{,yx} + w_{,y} w_{,yx} \right) \\
&\quad + \frac{1}{2} C_1 \otimes \left(u^0_{,yy} + v^0_{,xy} + w_{,xy} w_{,y} + w_{,x} w_{,yy} \right) \Bigg] w_{,x} + \Bigg[C_2 \otimes \left(u^0_{,xy} + w_{,x} w_{,xy} \right) + (C_1 + C_2) \otimes (v^0_{,yy} + w_{,y} w_{,yy}) \\
&\quad + \frac{1}{2} C_1 \otimes \left(u^0_{,yx} + v^0_{,xx} + w_{,xx} w_{,y} + w_{,x} w_{,yx} \right) \Bigg] w_{,y} + \Big[(C_1 + C_2) \otimes \left(u^0_{,x} + w^2_{,x}/2 \right) + C_2 \otimes \left(v^0_{,y} + w^2_{,y}/2 \right) \Big] w_{,xx} \\
&\quad + \Big[C_2 \otimes \left(u^0_{,x} + w^2_{,x}/2 \right) + (C_1 + C_2) \otimes \left(v^0_{,y} + w^2_{,y}/2 \right) \Big] w_{,yy} + C_1 \otimes \left(u^0_{,y} + v^0_{,x} + w_{,x} w_{,y} \right) w_{,xy} \Bigg\} = \rho h w_{,tt} - q, \\
&\frac{h^2}{6} (C_1 + C_2) \otimes \left(\varphi_{,xx} + C_2 \otimes \psi_{,yx} - \frac{h^2}{5} \beta D_{,x} \right) + \frac{h^2}{12} C_1 \otimes (\varphi_{,yy} + \psi_{,xy}) + C_1 \otimes (w_{,x} - \varphi) = \frac{\rho h^2}{6} \varphi_{,tt}, \\
&\frac{h^2}{6} \left(C_2 \otimes \varphi_{,xy} + (C_1 + C_2) \otimes \psi_{,yy} - \frac{h^2}{5} \beta D_{,y} \right) + \frac{h^2}{12} C_1 \otimes (\varphi_{,yx} + \psi_{,xx}) + C_1 \otimes (w_{,y} - \psi) = \frac{\rho h^2}{6} \psi_{,tt}.
\end{aligned}
\tag{11}
$$

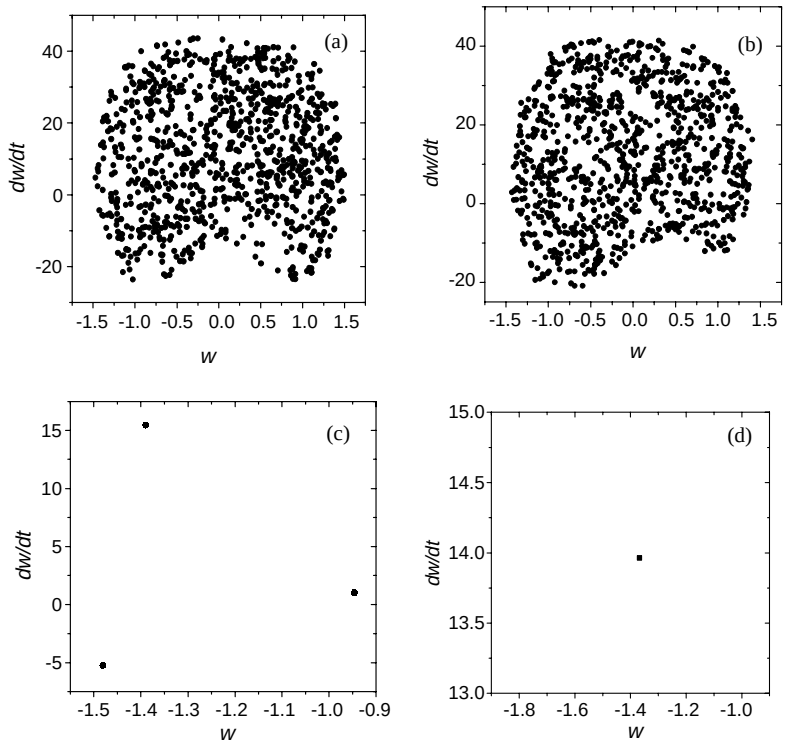

Fig. 9. Poincare sections of deflection for $\beta_1 = 10$, $q = 0.01$: (a) $\alpha = 0.02$, (b) $\alpha = 0.2$, (c) $\alpha = 5.0$, (d) $\alpha = 10.0$.

Clearly, Eqs. (11) are a system of nonlinear integro-partial-differential equations. In addition, we can also yield the differential equation of motion for the damage variable D as follows:

$$-\rho k\ddot{D} + \alpha D_{,\alpha\alpha} - \omega\dot{D} - \xi D - \frac{84\beta}{17h^2}(\varphi_{,x} + \psi_{,y}) = 0. \tag{12}$$

For convenience, it would be assumed that the edge of the plate is simply supported and the damage $D = 0$ along the edge of the plate, then the boundary conditions may be given as

$$\begin{aligned} &u^0 = v^0 = w = M_x = 0 \quad (x = 0, a), \\ &u^0 = v^0 = w = M_y = 0 \quad (y = 0, b), \\ &D = 0 \quad (x = 0, a) \quad \text{and} \quad (y = 0, b). \end{aligned} \tag{13}$$

Let the initial conditions be

$$\begin{aligned} &w|_{t=0} = w^0, \quad \dot{w}|_{t=0} = \dot{w}^0, \quad \varphi|_{t=0} = \varphi^0, \quad \dot{\varphi}|_{t=0} = \dot{\varphi}^0, \\ &\psi|_{t=0} = \psi^0, \quad \dot{\psi}|_{t=0} = \dot{\psi}^0, \quad D|_{t=0} = D^0, \quad \dot{D}|_{t=0} = \dot{D}^0. \end{aligned} \tag{14}$$

All the right-side functions in above equations are known functions of coordinates x_α only. Eqs. (11) and (12) and conditions (13) and (14) form the initial-boundary-value problem governing the dynamical behaviors of viscoelastic thick plates with damage. Due to that Eqs. (11) are a set of nonlinear integro-partial-differential equations, so it is difficult to obtain their solution. In order to solve the initial-boundary-

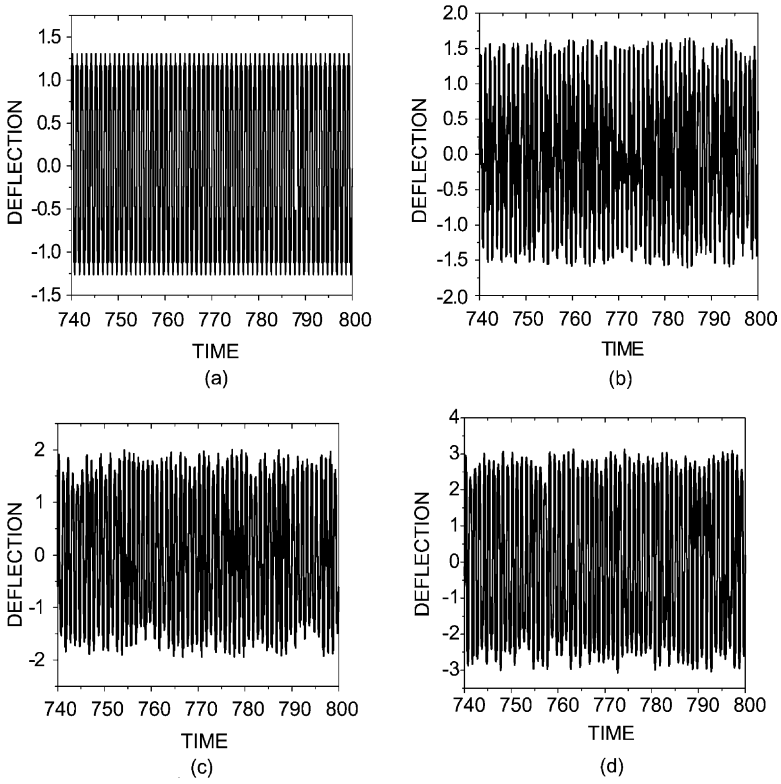

Fig. 10. Time-path curves of deflection for $\beta_1 = 10$, $\alpha = 0.2$: (a) $q = 0.0065$, (b) $q = 0.0066$, (c) $q = 0.01$, (d) $q = 0.03$.

value problem, we here apply the Galerkin method to simplify this problem. Observing the boundary conditions (13), the solution of Eqs. (11) and (12) may be taken in the forms as follows:

$$\begin{aligned}
u^0(x,y,t) &= \sum_{n=1}^{\infty}\sum_{m=1}^{\infty} \bar{u}^0(t)_{nm} \sin\frac{n\pi x}{a} \sin\frac{m\pi y}{b},\\
v^0(x,y,t) &= \sum_{n=1}^{\infty}\sum_{m=1}^{\infty} \bar{v}^0(t)_{nm} \sin\frac{n\pi x}{a} \sin\frac{m\pi y}{b},\\
w(x,y,t) &= \sum_{n=1}^{\infty}\sum_{m=1}^{\infty} \bar{w}(t)_{nm} \sin\frac{n\pi x}{a} \sin\frac{m\pi y}{b},\\
\varphi(x,y,t) &= \sum_{n=1}^{\infty}\sum_{m=1}^{\infty} \bar{\varphi}(t)_{nm} \cos\frac{n\pi x}{a} \sin\frac{m\pi y}{b},\\
\psi(x,y,t) &= \sum_{n=1}^{\infty}\sum_{m=1}^{\infty} \bar{\psi}(t)_{nm} \sin\frac{n\pi x}{a} \cos\frac{m\pi y}{b},\\
D(x,y,t) &= \sum_{n=1}^{\infty}\sum_{m=1}^{\infty} \overline{D}(t)_{nm} \sin\frac{n\pi x}{a} \sin\frac{m\pi y}{b}.
\end{aligned} \tag{15}$$

For convenience, it would be assumed that the transverse load q is given as

$$q(x,y,t) = \bar{q}(t) \sin\frac{\pi x}{a} \sin\frac{\pi y}{b}. \tag{16}$$

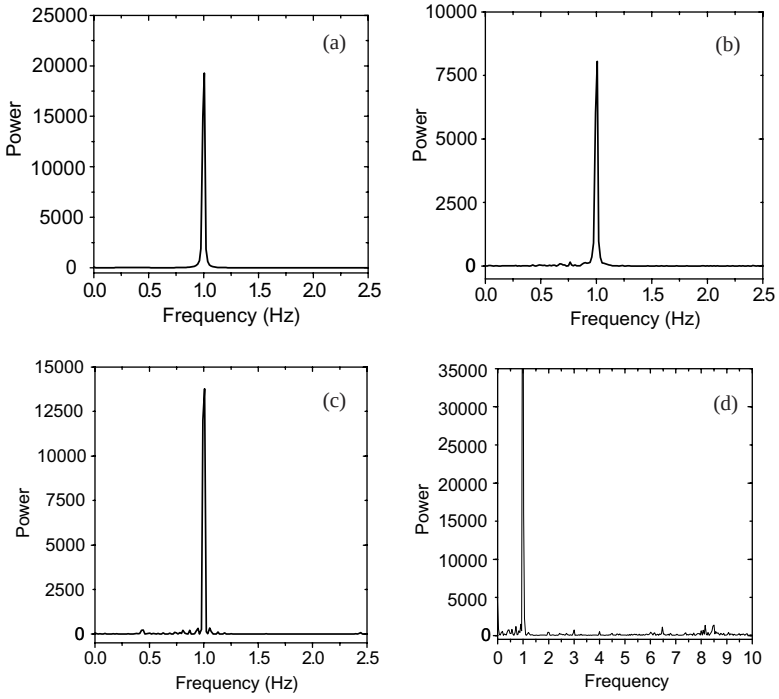

Fig. 11. Power spectrums of deflection for $\beta_1 = 10$, $\alpha = 0.2$: (a) $q = 0.0065$, (b) $q = 0.0066$, (c) $q = 0.01$, (d) $q = 0.03$.

Substituting (15) and (16) into (11) with $n = 1, 1$, $m = 1, 3$, we get the second-order Galerkin truncated model to be as

$$
\begin{aligned}
&A_1 \otimes \bar{u}_{11}^0 = 0 \quad A_2 \otimes \bar{u}_{13}^0 = 0,\\
&B_1 \otimes \bar{v}_{11}^0 = 0 \quad B_2 \otimes \bar{v}_{13}^0 = 0,\\
&A_3 \otimes \bar{w}_{11} + \bar{w}_{11}\left(A_4 \otimes \bar{w}_{11}^2\right) + \bar{w}_{11}\left[A_{41} \otimes \left(\bar{w}_{11}\bar{w}_{13}\right)\right] + \bar{w}_{11}\left(A_{42} \otimes \bar{w}_{13}^2\right) + \bar{w}_{13}\left(A_5 \otimes \bar{w}_{11}^2\right)\\
&\quad + \bar{w}_{13}\left[A_{51} \otimes \left(\bar{w}_{11}\bar{w}_{13}\right)\right] + A_6 \otimes \bar{\varphi}_{11} + A_7 \otimes \bar{\psi}_{11} = A_8\ddot{\bar{w}}_{11} - \frac{ab}{4}\bar{q},\\
&B_3 \otimes \bar{w}_{13} + \bar{w}_{11}\left(B_4 \otimes \bar{w}_{11}^2\right) + \bar{w}_{11}\left[B_{41} \otimes \left(\bar{w}_{11}\bar{w}_{13}\right)\right] + \bar{w}_{13}\left(B_5 \otimes \bar{w}_{13}^2\right) + B_6 \otimes \bar{\varphi}_{13} + B_7 \otimes \bar{\psi}_{13} = B_8\ddot{\bar{w}}_{13},\\
&A_9 \otimes \bar{w}_{11} + A_{10} \otimes \bar{\varphi}_{11} + A_{11} \otimes \bar{\psi}_{11} + A_{12}\overline{D}_{11} = A_{13}\ddot{\bar{\varphi}}_{11},\\
&B_9 \otimes \bar{w}_{13} + B_{10} \otimes \bar{\varphi}_{13} + B_{11} \otimes \bar{\psi}_{13} + B_{12}\overline{D}_{13} = B_{13}\ddot{\bar{\varphi}}_{13},\\
&A_{14} \otimes \bar{w}_{11} + A_{15} \otimes \bar{\varphi}_{11} + A_{16} \otimes \bar{\psi}_{11} + A_{17}\overline{D}_{11} = A_{18}\ddot{\bar{\psi}}_{11},\\
&B_{14} \otimes \bar{w}_{13} + B_{15} \otimes \bar{\varphi}_{13} + B_{16} \otimes \bar{\psi}_{13} + B_{17}\overline{D}_{13} = B_{18}\ddot{\bar{\psi}}_{13},\\
&A_{19}\overline{D}_{11} + A_{20}\dot{\overline{D}}_{11} + A_{21}\ddot{\overline{D}}_{11} + A_{22}\bar{\varphi}_{11} + A_{23}\bar{\psi}_{11} = 0,\\
&B_{19}\overline{D}_{13} + B_{20}\dot{\overline{D}}_{13} + B_{21}\ddot{\overline{D}}_{13} + B_{22}\bar{\varphi}_{13} + B_{23}\bar{\psi}_{13} = 0.
\end{aligned}
\tag{17}
$$

Coefficients in (17) are listed in Appendix A. If in (17), we set $\bar{w}_{13} = \bar{\varphi}_{13} = \bar{\psi}_{13} = 0$, that is, we take $n = 1$, $m = 1$, then the second-order Galerkin truncated model will degenerate into the first-order model. It can be seen that, from (17), the equations in u, v are uncoupled with w, D, φ, ψ.

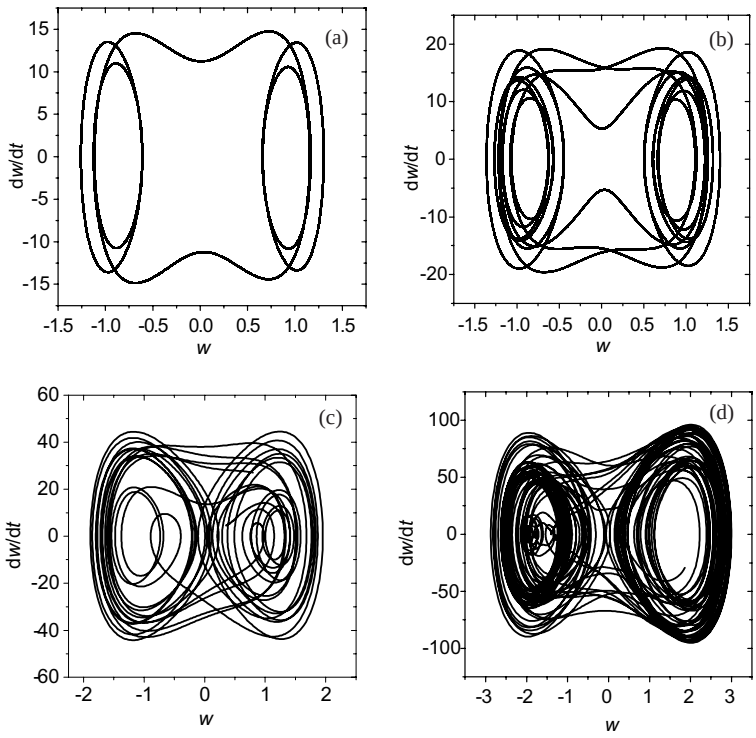

Fig. 12. Phase-trajectory diagrams of deflection for $\beta_1 = 10$: (a) $q = 0.0065$, (b) $q = 0.0066$, (c) $q = 0.01$, (d) $q = 0.03$.

3. Solution

Introduce the dimensionless parameters and the variable transformations as follows:

$$
\begin{aligned}
&\alpha_1 = a/b, \quad \beta_1 = b/h, \quad w = \bar{w}/h, \quad u = \bar{u}/h, \quad \upsilon = \bar{\upsilon}/h, \quad D_{11} = h^3\overline{D}_{11},\\
&D_{13} = h^3\overline{D}_{13}, \quad \beta_2 = C_1(0)/(\rho V_c^2), \quad \beta_3 = \beta/(\rho V_c^2), \quad \beta_4 = \alpha/(\rho k V_c^2),\\
&\beta_5 = \xi h^2/(\rho k V_c^2), \quad \beta_6 = \omega h/(\rho k V_c), \quad \beta_7 = \beta h^2/(\rho k V_c^2), \quad \tau = tV_c/h,\\
&\tau_0 = t_0 V_c/h, \quad c_1(\tau) = C_1(\tau)/C_1(0), \quad q_0 = \bar{q}/C_1(0),\\
&y_0 = t, \quad y_1 = w_{11}, \quad y_2 = \dot{w}_{11}, \quad y_3 = \varphi_{11}, \quad y_4 = \dot{\varphi}_{11}, \quad y_5 = \psi_{11}, \quad y_6 = \dot{\psi}_{11},\\
&y_7 = \int_0^t \dot{c}_1(t-\tau) w_{11}(\tau)\,\mathrm{d}\tau, \quad y_8 = \int_0^t \dot{c}_1(t-\tau)\varphi_{11}(\tau)\,\mathrm{d}\tau, \quad y_9 = \int_0^t \dot{c}_1(t-\tau)\psi_{11}(\tau)\,\mathrm{d}\tau,\\
&y_{10} = \int_0^t \dot{c}_1(t-\tau) w_{11}^2(\tau)\,\mathrm{d}\tau, \quad y_{11} = w_{13}, \quad y_{12} = \dot{w}_{13}, \quad y_{13} = \varphi_{13}, \quad y_{14} = \dot{\varphi}_{13}, \quad y_{15} = \psi_{13},\\
&y_{16} = \dot{\psi}_{13}, \quad y_{17} = \int_0^t \dot{c}_1(t-\tau) w_{13}(\tau)\,\mathrm{d}\tau, \quad y_{18} = \int_0^t \dot{c}_1(t-\tau) w_{13}^2(\tau)\,\mathrm{d}\tau,\\
&y_{19} = \int_0^t \dot{c}_1(t-\tau) w_{11}(\tau) w_{13}(\tau)\,\mathrm{d}\tau, \quad y_{20} = \int_0^t \dot{c}_1(t-\tau)\varphi_{13}(\tau)\,\mathrm{d}\tau, \quad y_{21} = \int_0^t \dot{c}_1(t-\tau)\psi_{13}(\tau)\,\mathrm{d}\tau,\\
&y_{22} = D_{11}, \quad y_{23} = D_{13}, \quad y_{24} = \dot{D}_{11}, \quad y_{25} = \dot{D}_{13}.
\end{aligned}
\tag{18}
$$

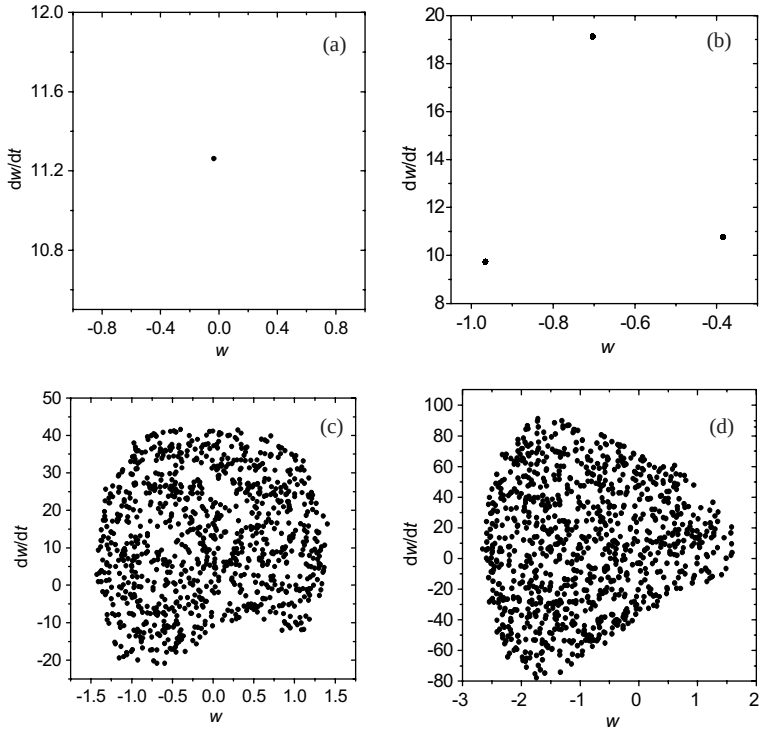

Fig. 13. Poincare sections of deflection for $\beta_1 = 10$: (a) $q = 0.0065$, (b) $q = 0.0066$, (c) $q = 0.01$, (d) $q = 0.03$.

For a standard linear solid material, the relaxation function is given as

$$\begin{aligned} &c_1(t) = c_0 + c_1 \exp(-\alpha t), \quad c_1(0) = c_0 + c_1 = 1, \\ &\dot{c}_1(t-\tau) = \Psi_1(t) \cdot \Psi_2(\tau) = -c_1 \exp(-\alpha t) \cdot \alpha \exp(\alpha \tau). \end{aligned} \tag{19}$$

Substituting (18) into (19) and (17) yields a set of ordinary differential equations

$$\dot{Y} = F(Y) \tag{20}$$

in which

$$Y = \{y_0, y_1, \ldots, y_{25}\}^{\mathrm{T}}, \quad F = \{F_0, F_1, \ldots, F_{25}\}^{\mathrm{T}}$$

and

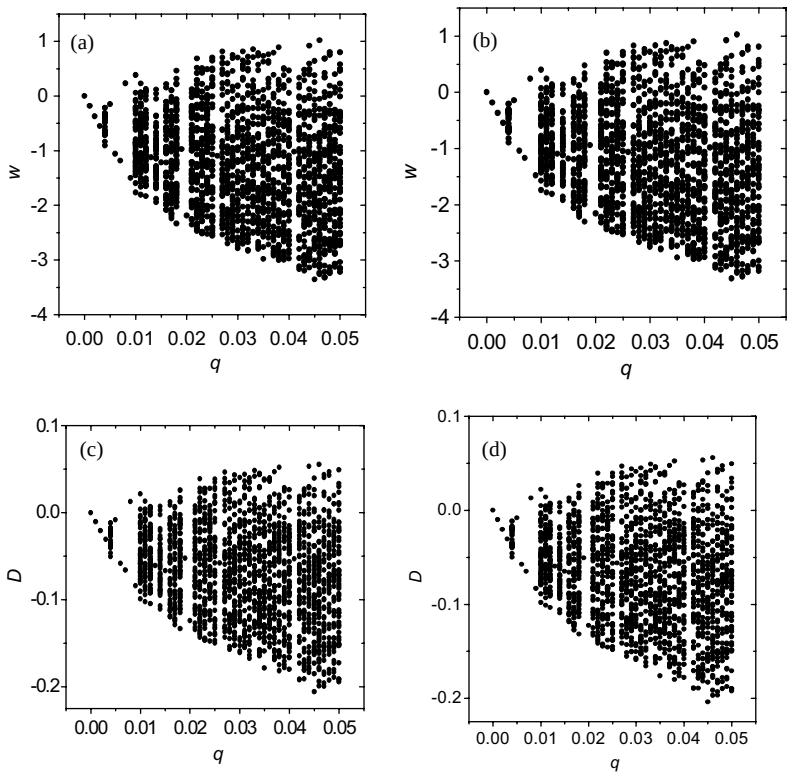

Fig. 14. Bifurcation figures of deflection for $\beta_1 = 10$, $\alpha = 0.2$: (a) first-order truncated system, (b) second-order truncated system, (c) first-order truncated system, (d) second-order truncated system.

$$
\begin{aligned}
&F_0 = 1, \quad F_1 = y_2,\\
&F_2 = k_1(y_1 + y_7) + k_2\left(y_1^3 + y_1y_{10}\right) + k_3\left(y_{11}^2y_1 + y_1y_{18}\right) + k_4\left(y_1^2y_{11} + y_1y_{19}\right) + k_5\left(y_1^2y_{11} + y_{10}y_{11}\right)\\
&\quad + k_6\left(y_1y_{11}^2 + y_{11}y_{19}\right) + k_7(y_3 + y_8) + k_{71}(y_5 + y_9) + \beta_2 q_0,\\
&F_3 = y_4, \quad F_4 = -k_{13}y_{22} + k_{14}(y_1 + y_7) - k_{15}(y_3 + y_8) - k_{151}(y_5 + y_9), \quad F_5 = y_6,\\
&F_6 = k_{191}(y_1 + y_7) - k_{192}(y_3 + y_8) - k_{193}(y_5 + y_9) - k_{194}y_{22},\\
&F_7 = -\alpha(c_1y_1 + y_7), \quad F_8 = -\alpha(c_1y_3 + y_8),\\
&F_9 = -\alpha(c_1y_5 + y_9), \quad F_{10} = -\alpha(c_1y_1^2 + y_{10}), \quad F_{11} = y_{12},\\
&F_{12} = -k_8(y_{11} + y_{17}) + k_9\left(y_1^2 + y_1y_{10}\right) + k_{10}\left(y_1^2y_{11} + y_1y_{19}\right) + k_{11}(y_{11}^3 + y_{11}y_{18}) + k_{12}(y_{13} + y_{20}),\\
&F_{13} = y_{14}, \quad F_{14} = -k_{16}y_{23} + k_{17}(y_{11} + y_{17}) - k_{18}(y_{13} + y_{20}),\\
&F_{15} = y_{16},\\
&F_{16} = k_{201}(y_{11} + y_{17}) - k_{202}(y_{13} + y_{20}) - k_{203}(y_{15} + y_{21}) - k_{204}y_{23},\\
&F_{17} = -\alpha(c_1y_{11} + y_{17}),\\
&F_{18} = -\alpha(c_1y_{11}^2 + y_{18}), \quad F_{19} = -\alpha(c_1y_1y_{13} + y_{19}), \quad F_{20} = -\alpha(c_1y_{13} + y_{20}),\\
&F_{21} = -\alpha(c_1y_{15} + y_{21}), \quad F_{22} = y_{24}, \quad F_{23} = y_{25},\\
&F_{24} = -k_{21}y_{22} - k_{22}y_{24} + k_{23}y_3 + k_{231}y_5,\\
&F_{25} = -k_{24}y_{23} - k_{25}y_{25} + k_{26}y_{13} + k_{261}y_{15}.
\end{aligned}
\tag{21}
$$

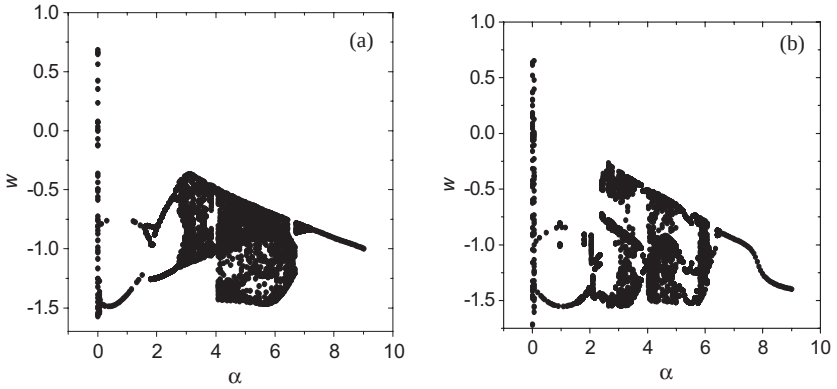

Fig. 15. Bifurcation figures of deflection for different load and $\beta_1 = 10$: (a) $q = 0.009$, (b) $q = 0.01$.

The coefficients in (21) are listed in Appendix B. In the above equations, we have assumed that Poisson ratio does not depend on time t, namely, $\mu(t) \equiv \mu = \text{const}$, so, $C_2(t)/C_1(t) = \mu/(1-\mu) = \mu_1$. From the initial conditions (14), it is clear that the initial values for (21) are given as

$$\begin{aligned}&\{(y_1(0), y_2(0), y_3(0), y_4(0), y_5(0), y_6(0), y_7(0), y_8(0), y_9(0), y_{10}(0), y_{11}(0), y_{12}(0), y_{13}(0), y_{14}(0), y_{15}(0), y_{16}(0),\\ &\quad y_{17}(0), y_{18}(0), y_{19}(0), y_{20}(0), y_{21}(0), y_{22}(0), y_{23}(0), y_{24}(0), y_{25}(0)\}\\ &\quad = \left\{w_1^0, \dot{w}_1^0, \varphi_1^0, \dot{\varphi}_1^0, \psi_1^0, \dot{\psi}_1^0, 0, 0, 0, 0, w_3^0, \dot{w}_3^0, \varphi_3^0, \dot{\varphi}_3^0, \psi_3^0, \dot{\psi}_3^0, 0, 0, 0, 0, 0, D_1^0, D_3^0, \dot{D}_1^0, \dot{D}_3^0\right\}. \end{aligned} \tag{22}$$

4. Numerical results and conclusions

Applying the variable Runge–Kutta–Merson method to the second-order Galerkin system (21) and (22), the corresponding history curves, power spectrums, phase diagrams, Poincare sections and bifurcation figures can all be obtained from the numerical methods in nonlinear dynamics. In numerical computation, we let $\alpha_1 = 1$, $\beta_2 = 10^5$, $\beta_3 = 6.67 \times 10^4$, $\beta_4 = 3.33 \times 10^5$, $\beta_5 = 5 \times 10^3$, $\beta_6 = 36.1$, $\beta_7 = 4.17 \times 10^3$, $\mu = 0.23$, $c_1 = 0.9$, $q_0 = q\sin(2\pi t)$, and further change the ratio of length to thickness β_1, material parameter α and load amplitude q. At the same time, the dynamic stabilities of the first-order and second-order truncated systems are studied and compared.

Fig. 1 shows that bifurcation figures of deflection, damage increment and rotation angles as the material parameter α increase and $\beta_1 = 10$. It could be seen that the dynamical behaviors of damage increment and rotation angles are similar to those of the deflection, so only dynamical diagrams of deflection will be demonstrated in the next analysis.

Various dynamic figures for given parameters are shown in Figs. 2–13, respectively. Figs. 2–5 show the time-path curves, power spectrums, phase-trajectory diagrams and Poincare sections for different ratio of length to thickness β_1 when $\alpha = 0.2$, $q = 0.2$. It can be seen that with the decrease of β_1 the system turns into stable period motions from unstable chaotic motions.

Figs. 6–9 show that the time-path curves, power spectrums, phase-trajectory diagrams and Poincare sections for different α when $q = 0.01$, $\beta_1 = 10$. It can be seen that with the increase α the system turns into stable period motions from unstable chaotic motions.

Figs. 10–13 show the time-path curves, power spectrums, phase-trajectory diagrams and Poincare sections for different values of the load parameter q when $\beta_1 = 10$, $\alpha = 0.2$. It is easily seen that the increase of q will help that the motion states transfer into unstable chaotic motions from stable periodic motions.

Fig. 14 shows the bifurcations of deflection of the first-order and second-order systems with the increase of the load parameter q when $\beta_1 = 10$, $\alpha = 0.2$. It could be seen from Fig. 14 that the dynamic behaviors for the first-order and second-order truncated systems are the same qualitatively.

Fig. 15 shows the bifurcation figures of deflection of the second-order truncated system with the increase of the material parameter α under different load parameters when $\beta_1 = 10$. It could be seen that bifurcation figures are far from others for small difference of q. This indicates that the increase of α will help to the stability of the viscoelastic plates with damage.

5. Discussion

5.1. Dynamical behaviors of viscoelastic plates with damage under small deformations

If the deformation of the plate is small, then the plate will be in stable period motions. In this case Eqs. (3) becomes as

$$\varepsilon_{ij} = \frac{1}{2}(u_{i,j} + u_{j,i}).$$

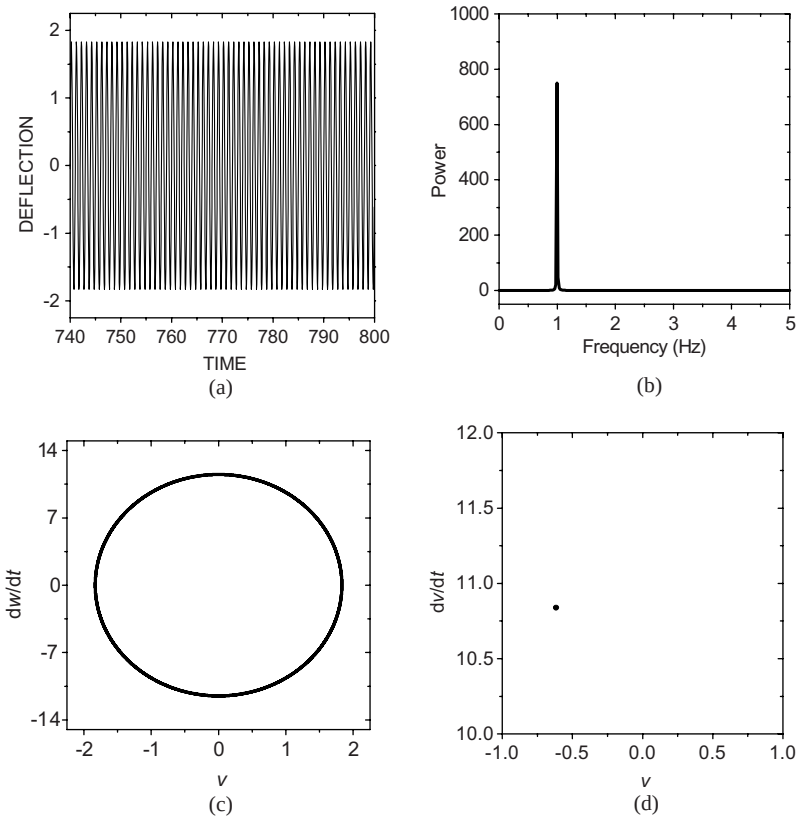

Fig. 16. Dynamic property figures for $\alpha = 0.2$, $q = 0.2$, $\beta_1 = 4.2$: (a) time-path curves, (b) power spectrum, (c) phase-trajectory diagram, (d) Poincare section.

We may still discuss the dynamical properties of the linear dynamical systems by the above method. Fig. 16 shows the time-path curve, power spectrum, phase-trajectory diagram and Poincare section for the linear dynamic system when $\alpha = 0.2$, $q = 0.2$, $\beta_1 = 4.2$. It can be seen that the linear system is stable period

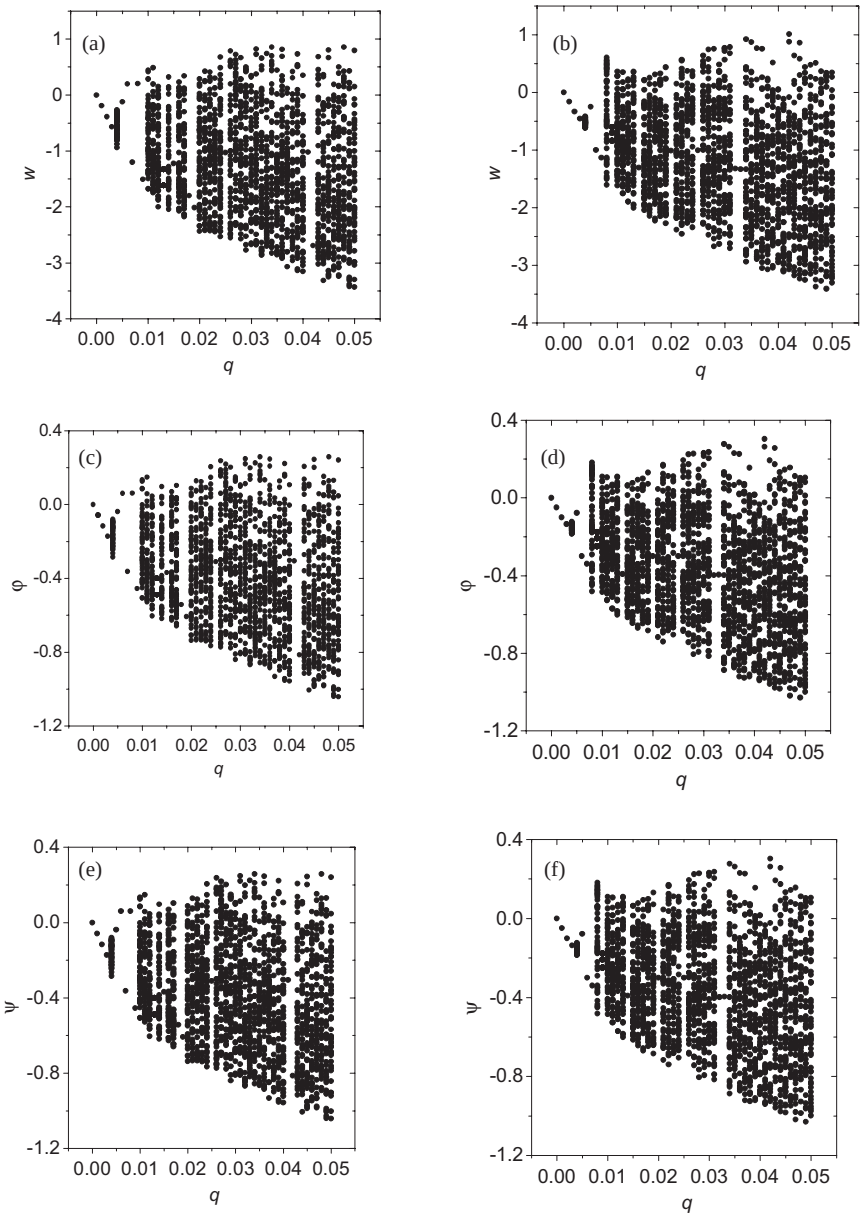

Fig. 17. Bifurcation figures of deflection and rotation of plates without damage: (a) bifurcation of deflection without damage, (b) bifurcation of deflection with damage, (c) bifurcation of rotation φ without damage, (d) bifurcation of rotation φ with damage, (e) bifurcation of rotation ψ without damage, (f) bifurcation of rotation ψ without damage.

motion but under the case of the same parameter the nonlinear system will be chaotic motion as shown Figs. 2(a)–5(a).

5.2. Comparison between dynamical properties of plates with damage and without damage

In the section, we consider the effects of damage on dynamical properties of viscoelastic thick plates. For plates with damage, we take the damage parameters $\beta_3 = 1.334 \times 10^5$, $\beta_7 = 8.34 \times 10^3$, the others material parameters are the same as those in the above section. For plates without damage, we have to only let $\beta_3 = \beta_4 = \beta_5 = \beta_6 = \beta_7 = 0$ in the above parameters (please see Eqs. (12) and (18)). Fig. 17 shows the bifurcation figures of deflection and rotation angles of plates without damage or with damage. It can be seen that the chaos in the plates without damage will appear when the loading parameter $q \approx 0.01$, while the chaos in the plates with damage appear when loading parameter $q \approx 0.008$. In the other word, chaos may appear in advance when there is damage in plates.

Fig. 18 shows the dynamical properties of viscoelastic thick plates with or without damage when $\beta_1 = 10$, $\alpha = 0.2$, $q = 0.008$ and $\beta_3 = 1.334 \times 10^5$, $\beta_7 = 8.34 \times 10^3$ (β_3, β_7 are twice damage parameters in Figs. 1–16) and the other material parameters are the same as those by given before. One can see that when $q = 0.008$, the motion of the viscoelastic plates with damage will be chaotic but the motion of plates without damage is still stable. Hence, it is possible that damage makes the dynamical properties of plate become unstable, and so it is harmful to the stability of structures. We have to decrease the material parameters β_3 and β_7 to ensure the stability of structures.

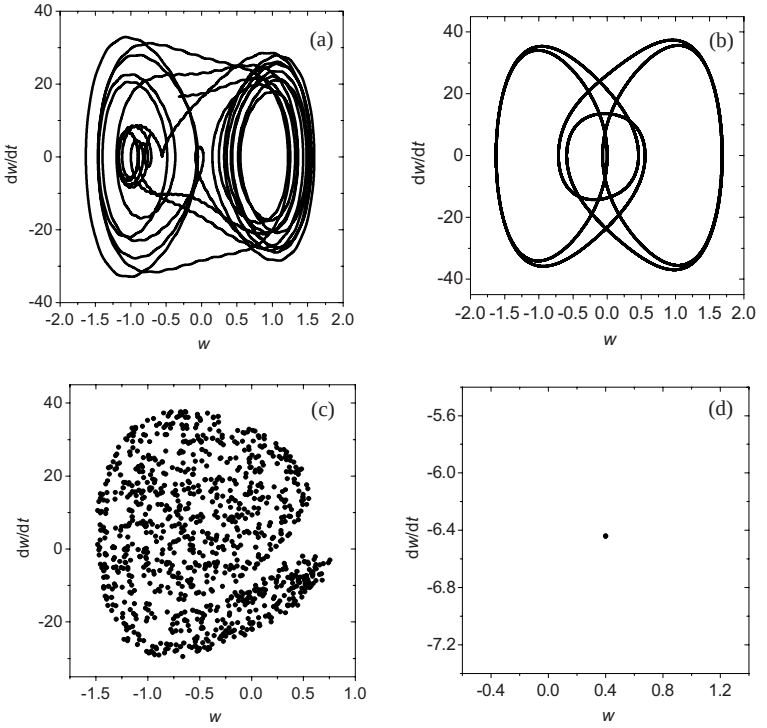

Fig. 18. Comparing of dynamical properties of plates with damage and without damage: (a) phase-trajectory diagram of deflection with damage, (b) phase-trajectory diagram of deflection without damage, (c) Poincare section of deflection with damage, (d) Poincare section of deflection without damage.

Acknowledgements

This project was supported by the National Natural Science Foundation of China (10272069) and the Shanghai Key Subject Program.

Appendix A

$$A_1 = -\pi^2 b(C_1 + C_2)/(4a) - \pi^2 a C_1/(8b), \quad A_2 = -9\pi^2 a C_1/(8b) - \pi^2 b(C_1 + C_2)/(4a),$$

$$B_1 = -\pi^2 b C_1/(8a) - \pi^2 a(C_1 + C_2)/(4b), \quad B_2 = -9\pi^2 a(C_1 + C_2)/(4b) - \pi^2 b C_1/(8a),$$

$$A_3 = h\pi^2[-a/(8b) - b/(8a)]C_1,$$

$$A_4 = h\pi^4[-9a(C_1 + C_2)/(128b^3) - C_1/(64ab) - 3b(C_1 + C_2)/(64a^3) + C_2/(128ab)],$$

$$A_{41} = h\pi^4[-9a(C_1 + C_2)/(64b^3) + C_1/(32ab) + b(C_1 + C_2)/(32a^3) - 7C_2/(64ab)],$$

$$A_{42} = h\pi^4[-27a(C_1 + C_2)/(64b^3) - b(C_1 + C_2)/(32a^3) + 17C_2/(64ab)],$$

$$A_5 = h\pi^4[-9a(C_1 + C_2)/(128b^3) + bC_1/(64a^3) + b(C_1 + C_2)/(64a^3) + 5C_2/(128ab)],$$

$$A_{51} = h\pi^4[-27a(C_1 + C_2)/(32b^3) - 5C_1/(32ab) - b(C_1 + C_2)/(16a^3)],$$

$$A_6 = B_6 = h\pi b C_1/8, \quad A_7 = h\pi a C_1/8, \quad B_7 = 3h\pi a C_1/8, \quad A_8 = B_8 = \rho hab/4,$$

$$B_3 = h\pi^2[-9a/(8b) - b/(8a)]C_1,$$

$$B_4 = h\pi^4[-9a(C_1 + C_2)/(128b^3) + C_1/(64ab) + b(C_1 + C_2)/(64a^3) + 5C_2/(128ab)],$$

$$B_{41} = h\pi^4[-27a(C_1 + C_2)/32b^3 - 5C_1/(32ab) - b(C_1 + C_2)/(16a^3)],$$

$$B_5 = h\pi^4[-783a(C_1 + C_2)/(128b^3) - 9C_1/(64ab) - 5b(C_1 + C_2)/(64a^3) - 5C_2/(128ab)],$$

$$A_9 = B_9 = \pi b C_1/4,$$

$$A_{10} = -abC_1/4 - \pi^2 a h^2 C_1/(48b) - \pi^2 b h^2(C_1 + C_2)/(24a),$$

$$A_{11} = A_{15} = -\pi^2 h^2(C_1 + 2C_2)/48, \quad B_{11} = B_{15} = -\pi^2 h^2(C_1 + 2C_2)/16,$$

$$A_{12} = B_{12} = -\pi b\beta h^4/120, \quad A_{13} = B_{13} = \rho abh^2/24,$$

$$B_{10} = -abC_1/4 - 3\pi^2 a h^2 C_1/(16b) - \pi^2 b h^2(C_1 + C_2)/(24a),$$

$$A_{14} = \pi a C_1/4, \quad B_{14} = 3\pi a C_1/4,$$

$$A_{16} = -abC_1/4 - \pi^2 a h^2(C_1 + C_2)/(24b) - \pi^2 b h^2 C_1/(48a),$$

$$B_{16} = -abC_1/4 - 3\pi^2 a h^2(C_1 + C_2)/(8b) - \pi^2 b h^2 C_1/(48a),$$

$$A_{17} = -\pi a\beta h^4/120, \quad B_{17} = -\pi a\beta h^4/40, \quad A_{18} = B_{18} = \rho abh^2/24,$$

$$A_{19} = -\pi^2 a\alpha/(4b) - \pi^2 b\alpha/(4a) - ab\xi/4,$$

$$A_{20} = B_{20} = -ab\omega/4, \quad A_{21} = B_{21} = -ab\rho k/4,$$

$$A_{22} = B_{22} = 21\pi b\beta/(17h^2), \quad A_{23} = 21, \pi a\beta/(17h^2), \quad B_{23} = 63\pi a\beta/(17h^2),$$

$$B_{19} = -9\pi^2 a\alpha/(4b) - \pi^2 b\alpha/(4a) - ab\xi/4.$$

Appendix B

$$
\begin{aligned}
&k_1 = -\pi^2\beta_2(1+\alpha_1^2)/(2\alpha_1^2\beta_1^2),\\
&k_2 = \pi^4\beta_2\big[-9(1+\mu_1)\alpha_1^4 + (-2+\mu_1)\alpha_1^2 - 6(1+\mu_1)\big]/\big(32\alpha_1^4\beta_1^4\big),\\
&k_3 = \pi^4\beta_2\big[-27(1+\mu_1)\alpha_1^4 + 17\mu_1\alpha_1^2 - 2(1+\mu_1)\big]/\big(16\alpha_1^4\beta_1^4\big),\\
&k_4 = \pi^4\beta_2\big[-9(1+\mu_1)\alpha_1^4 + (2-7\mu_1)\alpha_1^2 + 2(1+\mu_1)\big]/\big(16\alpha_1^4\beta_1^4\big),\\
&k_5 = \pi^4\beta_2\big[-9(1+\mu_1)\alpha_1^4 + 5\mu_1\alpha_1^2 + 2(2+\mu_1)\big]/\big(32\alpha_1^4\beta_1^4\big),\\
&k_6 = \pi^4\beta_2\big[-27(1+\mu_1)\alpha_1^4 - 5\alpha_1^2 - 2(1+\mu_1)\big]/\big(8\alpha_1^4\beta_1^4\big),\\
&k_7 = \pi\beta_2/(2\alpha_1\beta_1), \quad k_{71} = \pi\beta_2/(2\beta_1), \quad k_8 = \pi^2\beta_2\big(1+9\alpha_1^2\big)/\big(2\alpha_1^2\beta_1^2\big),\\
&k_9 = \pi^4\beta_2\big[-9(1+\mu_1)\alpha_1^4 + (2+5\mu_1)\alpha_1^2 + 2(1+\mu_1)\big]/\big(32\alpha_1^4\beta_1^4\big),\\
&k_{10} = \pi^4\beta_2\big[-27(1+\mu_1)\alpha_1^4 - 5\alpha_1^2 - 2(1+\mu_1)\big]/\big(8\alpha_1^4\beta_1^4\big),\\
&k_{11} = \pi^4\beta_2\big[-783(1+\mu_1)\alpha_1^4 - (18+5\mu_1)\alpha_1^2 - 10(1+\mu_1)\big]/\big(32\alpha_1^4\beta_1^4\big),\\
&k_{12} = \pi\beta_2/(2\alpha_1\beta_1), \quad k_{13} = \pi\beta_3/(5\alpha_1\beta_1), \quad k_{14} = 6\pi\beta_2/(\alpha_1\beta_1),\\
&k_{15} = 6\beta_2 + \pi^2\beta_2/(2\beta_1^2) + \pi^2\beta_2(1+\mu_1)/\big(\alpha_1^2\beta_1^2\big),\\
&k_{151} = \pi^2\beta_2(1+2\mu_1)/\big(2\alpha_1\beta_1^2\big), \quad k_{16} = \pi\beta_3/(5\alpha_1\beta_1), \quad k_{17} = 6\pi\beta_2/(\alpha_1\beta_1),\\
&k_{18} = 6\beta_2 + 9\pi^2\beta_2/(2\beta_1^2) + \pi^2\beta_2(1+\mu_1)/(\alpha_1^2\beta_1^2),\\
&k_{191} = 6\pi\beta_2/\beta_1, \quad k_{192} = \pi^2\beta_2(1+2\mu_1)/\big(2\alpha_1\beta_1^2\big),\\
&k_{193} = 6\beta_2 + \pi^2\beta_2(1+\mu_1)/\beta_1^2 + \pi^2\beta_2/\big(2\alpha_1^2\beta_1^2\big), \quad k_{194} = \pi\beta_3/(5\beta_1),\\
&k_{201} = 18\pi\beta_2/\beta_1, \quad k_{202} = 3\pi^2\beta_2(1+2\mu_1)/\big(2\alpha_1\beta_1^2\big),\\
&k_{203} = 6\beta_2 + 9\pi^2\beta_2(1+\mu_1)/\beta_1^2 + \pi^2\beta_2/\big(2\alpha_1^2\beta_1^2\big), \quad k_{204} = 3\pi\beta_3/(5\beta_1),\\
&k_{21} = \pi^2\beta_4\big(1+\alpha_1^2\big)/\big(\alpha_1^2\beta_1^2\big) + \beta_5, \quad k_{22} = k_{25} = \beta_6,\\
&k_{23} = k_{26} = 84\pi\beta_7/(17\alpha_1\beta_1), \quad k_{231} = 84\pi\beta_7/(17\beta_1),\\
&k_{24} = \pi^2\beta_4\big(1+9\alpha_1^2\big)/\big(\alpha_1^2\beta_1^2\big) + \beta_5, \quad k_{261} = 252\pi\beta_7/(17\beta_1).
\end{aligned}
$$

References

Argyris, J., 1996. Chaotic vibrations of a nonlinear viscoelastic beam. Chaos Solit. Fract. 7, 151–163.

Cederbaum, G., Aboudi, J., 1991. Dynamic instability of shear-deformable viscoelastic laminated plates by Lyapunov exponents. Int. J. Solid Struct. 28, 317–327.

Cederbaum, G., Mond, M., 1992. Stability properties of a viscoelastic column under a period force. J. Appl. Mech. 59, 16–19.

Cederbaum, G., Drawshi, M., 1994. Multiple equilibrium states in the analysis of viscoelastic nonlinear circular plates. Int. J. Mech. Sci. 36, 149–155.

Cheng, C.-j., Zhang, N.-h., 1998. Chaotic and hyperchaotic behavior of viscoelastic rectangular plates under a transverse periodic load. Acta Mech. Sini. 30, 690–699 (in Chinese).

Cheng, C.-j., Zhu, Z.-y., 1991. Buckling and Bifurcation in Structures. Lanzhou University Press, Lanzhou (in Chinese).

Cowin, S.C., Nunziato, J.W., 1983. Linear theory materials with voids. J. Elast. 13, 125–147.

Ding, R., Zhu, Z.-y., Cheng, C.-j., 1998. Dynamic properties of viscoelastic plates. In: Chien, W.-Z. (Ed.), Proc. of the 3rd Inter. Conf. on Nonlinear Mech.. Shanghai Univ. Press, Shanghai, pp. 185–190.

Drozdov, A., 1993. Stability of viscoelastic shell under periodic and stochastic loading. Mech. Res. Commun. 20, 481–486.

Li, J.-j., Cheng, C.-j., Zhang, N.-h., 2002. Dynamical stability of viscoelastic plates with finite deformation and shear effects. J. Shanghai Univ. 6, 115–124.

Parker, T.S., Chua, L.O., 1989. Practical Numerical Algorithms for Chaotic Systems. Springer-Verlag, New York.

Suire, G., Cederbaum, G., 1995. Periodic and chaotic behavior of viscoelastic nonlinear bars under harmonic excitations. Int. J. Mech. Sci. 37, 753–772.

Touati, D., Cederbaum, G., 1995. Influence of large deflections on the dynamic stability of nonlinear viscoelastic plates. Acta Mech. 113, 215–231.

Tylikowski, A., 1989. Dynamic stability of viscoelastic shell under time-dependent membrane loads. Int. J. Mech. Sci. 31, 591–597.

Zhu, Y.-y., Zhang, N.-h., Miura, F., 1998. Dynamical behavior of viscoelastic rectangular plates. In: Chien, W.-Z. (Ed.), Proc. of the 3rd Inter. Conf. on Nonlinear Mech. Shanghai Univ. Press, Shanghai, pp. 445–450.